

Measurements of the τ mass and the mass difference of the τ^+ and τ^- at BABAR

B. Aubert,¹ Y. Karyotakis,¹ J. P. Lees,¹ V. Poireau,¹ E. Prencipe,¹ X. Prudent,¹ V. Tisserand,¹ J. Garra Tico,² E. Grauges,² M. Martinelli,^{3a,3b} A. Palano,^{3a,3b} M. Pappagallo,^{3a,3b} G. Eigen,⁴ B. Stugu,⁴ L. Sun,⁴ M. Battaglia,⁵ D. N. Brown,⁵ L. T. Kerth,⁵ Yu. G. Kolomensky,⁵ G. Lynch,⁵ I. L. Osipenkov,⁵ K. Tackmann,⁵ T. Tanabe,⁵ C. M. Hawkes,⁶ N. Soni,⁶ A. T. Watson,⁶ H. Koch,⁷ T. Schroeder,⁷ D. J. Asgeirsson,⁸ B. G. Fulsom,⁸ C. Hearty,⁸ T. S. Mattison,⁸ J. A. McKenna,⁸ M. Barrett,⁹ A. Khan,⁹ A. Randle-Conde,⁹ V. E. Blinov,¹⁰ A. D. Bukin,^{10,*} A. R. Buzykaev,¹⁰ V. P. Druzhinin,¹⁰ V. B. Golubev,¹⁰ A. P. Onuchin,¹⁰ S. I. Serednyakov,¹⁰ Yu. I. Skovpen,¹⁰ E. P. Solodov,¹⁰ K. Yu. Todyshev,¹⁰ M. Bondioli,¹¹ S. Curry,¹¹ I. Eschrich,¹¹ D. Kirkby,¹¹ A. J. Lankford,¹¹ P. Lund,¹¹ M. Mandelkern,¹¹ E. C. Martin,¹¹ D. P. Stoker,¹¹ H. Atmacan,¹² J. W. Gary,¹² F. Liu,¹² O. Long,¹² G. M. Vitug,¹² Z. Yasin,¹² V. Sharma,¹³ C. Campagnari,¹⁴ T. M. Hong,¹⁴ D. Kovalskiy,¹⁴ M. A. Mazur,¹⁴ J. D. Richman,¹⁴ T. W. Beck,¹⁵ A. M. Eisner,¹⁵ C. A. Heusch,¹⁵ J. Kroseberg,¹⁵ W. S. Lockman,¹⁵ A. J. Martinez,¹⁵ T. Schalk,¹⁵ B. A. Schumm,¹⁵ A. Seiden,¹⁵ L. Wang,¹⁵ L. O. Winstrom,¹⁵ C. H. Cheng,¹⁶ D. A. Doll,¹⁶ B. Echenard,¹⁶ F. Fang,¹⁶ D. G. Hitlin,¹⁶ I. Narsky,¹⁶ P. Ongmongkolku,¹⁶ T. Piatenko,¹⁶ F. C. Porter,¹⁶ R. Andreassen,¹⁷ G. Mancinelli,¹⁷ B. T. Meadows,¹⁷ K. Mishra,¹⁷ M. D. Sokoloff,¹⁷ P. C. Bloom,¹⁸ W. T. Ford,¹⁸ A. Gaz,¹⁸ J. F. Hirschauer,¹⁸ M. Nagel,¹⁸ U. Nauenberg,¹⁸ J. G. Smith,¹⁸ S. R. Wagner,¹⁸ R. Ayad,^{19,†} W. H. Toki,¹⁹ R. J. Wilson,¹⁹ E. Feltresi,²⁰ A. Hauke,²⁰ H. Jasper,²⁰ T. M. Karbach,²⁰ J. Merkel,²⁰ A. Petzold,²⁰ B. Spaan,²⁰ K. Wacker,²⁰ M. J. Kobel,²¹ R. Nogowski,²¹ K. R. Schubert,²¹ R. Schwierz,²¹ D. Bernard,²² E. Latour,²² M. Verderi,²² P. J. Clark,²³ S. Playfer,²³ J. E. Watson,²³ M. Andreotti,^{24a,24b} D. Bettoni,^{24a} C. Bozzi,^{24a} R. Calabrese,^{24a,24b} A. Cecchi,^{24a,24b} G. Cibinetto,^{24a,24b} E. Fioravanti,^{24a,24b} P. Franchini,^{24a,24b} E. Luppi,^{24a,24b} M. Munerato,^{24a,24b} M. Negrini,^{24a,24b} A. Petrella,^{24a,24b} L. Piemontese,^{24a} V. Santoro,^{24a,24b} R. Baldini-Ferrolì,²⁵ A. Calcaterra,²⁵ R. de Sangro,²⁵ G. Finocchiaro,²⁵ S. Pacetti,²⁵ P. Patteri,²⁵ I. M. Peruzzi,^{25,‡} M. Piccolo,²⁵ M. Rama,²⁵ A. Zallo,²⁵ R. Contri,^{26a,26b} E. Guido,^{26a,26b} M. Lo Vetere,^{26a,26b} M. R. Monge,^{26a,26b} S. Passaggio,^{26a} C. Patrignani,^{26a,26b} E. Robutti,^{26a} S. Tosi,^{26a,26b} K. S. Chaisanguanthum,²⁷ M. Morii,²⁷ A. Adametz,²⁸ J. Marks,²⁸ S. Schenk,²⁸ U. Uwer,²⁸ F. U. Bernlochner,²⁹ V. Klose,²⁹ H. M. Lacker,²⁹ T. Lueck,²⁹ A. Volk,²⁹ D. J. Bard,³⁰ P. D. Dauncey,³⁰ M. Tibbetts,³⁰ P. K. Behera,³¹ M. J. Charles,³¹ U. Mallik,³¹ J. Cochran,³² H. B. Crawley,³² L. Dong,³² V. Eyges,³² W. T. Meyer,³² S. Prell,³² E. I. Rosenberg,³² A. E. Rubin,³² Y. Y. Gao,³³ A. V. Gritsan,³³ Z. J. Guo,³³ N. Arnaud,³⁴ J. Béquilleux,³⁴ A. D'Orazio,³⁴ M. Davier,³⁴ D. Derkach,³⁴ J. Firmino da Costa,³⁴ G. Grosdidier,³⁴ F. Le Diberder,³⁴ V. Lepeltier,³⁴ A. M. Lutz,³⁴ B. Malaescu,³⁴ S. Pruvot,³⁴ P. Roudeau,³⁴ M. H. Schune,³⁴ J. Serrano,³⁴ V. Sordini,^{34,§} A. Stocchi,³⁴ G. Wormser,³⁴ D. J. Lange,³⁵ D. M. Wright,³⁵ I. Bingham,³⁶ J. P. Burke,³⁶ C. A. Chavez,³⁶ J. R. Fry,³⁶ E. Gabathuler,³⁶ R. Gamet,³⁶ D. E. Hutchcroft,³⁶ D. J. Payne,³⁶ C. Touramanis,³⁶ A. J. Bevan,³⁷ C. K. Clarke,³⁷ F. Di Lodovico,³⁷ R. Sacco,³⁷ M. Sigamani,³⁷ G. Cowan,³⁸ S. Paramesvaran,³⁸ A. C. Wren,³⁸ D. N. Brown,³⁹ C. L. Davis,³⁹ A. G. Denig,⁴⁰ M. Fritsch,⁴⁰ W. Gradl,⁴⁰ A. Hafner,⁴⁰ K. E. Alwyn,⁴¹ D. Bailey,⁴¹ R. J. Barlow,⁴¹ G. Jackson,⁴¹ G. D. Lafferty,⁴¹ T. J. West,⁴¹ J. I. Yi,⁴¹ J. Anderson,⁴² C. Chen,⁴² A. Jawahery,⁴² D. A. Roberts,⁴² G. Simi,⁴² J. M. Tuggle,⁴² C. Dallapiccola,⁴³ E. Salvati,⁴³ R. Cowan,⁴⁴ D. Dujmic,⁴⁴ P. H. Fisher,⁴⁴ S. W. Henderson,⁴⁴ G. Sciolla,⁴⁴ M. Spitznagel,⁴⁴ R. K. Yamamoto,⁴⁴ M. Zhao,⁴⁴ P. M. Patel,⁴⁵ S. H. Robertson,⁴⁵ M. Schram,⁴⁵ P. Biassoni,^{46a,46b} A. Lazzaro,^{46a,46b} V. Lombardo,^{46a} F. Palombo,^{46a,46b} S. Stracka,^{46a,46b} L. Cremaldi,⁴⁷ R. Godang,^{47,||} R. Kroeger,⁴⁷ P. Sonnek,⁴⁷ D. J. Summers,⁴⁷ H. W. Zhao,⁴⁷ M. Simard,⁴⁸ P. Taras,⁴⁸ H. Nicholson,⁴⁹ G. De Nardo,^{50a,50b} L. Lista,^{50a} D. Monorchio,^{50a,50b} G. Onorato,^{50a,50b} C. Sciacca,^{50a,50b} G. Raven,⁵¹ H. L. Snoek,⁵¹ C. P. Jessop,⁵² K. J. Knoepfel,⁵² J. M. LoSecco,⁵² W. F. Wang,⁵² L. A. Corwin,⁵³ K. Honscheid,⁵³ H. Kagan,⁵³ R. Kass,⁵³ J. P. Morris,⁵³ A. M. Rahimi,⁵³ S. J. Sekula,⁵³ Q. K. Wong,⁵³ N. L. Blount,⁵⁴ J. Brau,⁵⁴ R. Frey,⁵⁴ O. Igonkina,⁵⁴ J. A. Kolb,⁵⁴ M. Lu,⁵⁴ R. Rahmat,⁵⁴ N. B. Sinev,⁵⁴ D. Strom,⁵⁴ J. Strube,⁵⁴ E. Torrence,⁵⁴ G. Castelli,^{55a,55b} N. Gagliardi,^{55a,55b} M. Margoni,^{55a,55b} M. Morandin,^{55a} M. Posocco,^{55a} M. Rotondo,^{55a} F. Simonetto,^{55a,55b} R. Stroili,^{55a,55b} C. Voci,^{55a,55b} P. del Amo Sanchez,⁵⁶ E. Ben-Haim,⁵⁶ G. R. Bonneaud,⁵⁶ H. Briand,⁵⁶ J. Chauveau,⁵⁶ O. Hamon,⁵⁶ Ph. Leruste,⁵⁶ G. Marchiori,⁵⁶ J. Ocariz,⁵⁶ A. Perez,⁵⁶ J. Prendki,⁵⁶ S. Sitt,⁵⁶ L. Gladney,⁵⁷ M. Biasini,^{58a,58b} E. Manoni,^{58a,58b} C. Angelini,^{59a,59b} G. Batignani,^{59a,59b} S. Bettarini,^{59a,59b} G. Calderini,^{59a,59b,¶} M. Carpinelli,^{59a,59b,**} A. Cervelli,^{59a,59b} F. Forti,^{59a,59b} M. A. Giorgi,^{59a,59b} A. Lusiani,^{59a,59c} M. Morganti,^{59a,59b} N. Neri,^{59a,59b} E. Paoloni,^{59a,59b} G. Rizzo,^{59a,59b} J. J. Walsh,^{59a} D. Lopes Pegna,⁶⁰ C. Lu,⁶⁰ J. Olsen,⁶⁰ A. J. S. Smith,⁶⁰ A. V. Telnov,⁶⁰ F. Anulli,^{61a} E. Baracchini,^{61a,61b} G. Cavoto,^{61a} R. Faccini,^{61a,61b} F. Ferrarotto,^{61a} F. Ferroni,^{61a,61b} M. Gaspero,^{61a,61b} P. D. Jackson,^{61a} L. Li Gioi,^{61a} M. A. Mazzoni,^{61a} S. Morganti,^{61a} G. Piredda,^{61a} F. Renga,^{61a,61b} C. Voena,^{61a} M. Ebert,⁶² T. Hartmann,⁶² H. Schröder,⁶² R. Waldi,⁶² T. Adye,⁶³ B. Franek,⁶³ E. O. Olaiya,⁶³ F. F. Wilson,⁶³ S. Emery,⁶⁴ L. Esteve,⁶⁴ G. Hamel de Monchenault,⁶⁴ W. Kozanecki,⁶⁴ G. Vasseur,⁶⁴ Ch. Yèche,⁶⁴ M. Zito,⁶⁴ M. T. Allen,⁶⁵ D. Aston,⁶⁵ R. Bartoldus,⁶⁵ J. F. Benitez,⁶⁵ R. Cenci,⁶⁵ J. P. Coleman,⁶⁵

M. R. Convery,⁶⁵ J. C. Dingfelder,⁶⁵ J. Dorfan,⁶⁵ G. P. Dubois-Felsmann,⁶⁵ W. Dunwoodie,⁶⁵ R. C. Field,⁶⁵ M. Franco Sevilla,⁶⁵ A. M. Gabareen,⁶⁵ M. T. Graham,⁶⁵ P. Grenier,⁶⁵ C. Hast,⁶⁵ W. R. Innes,⁶⁵ J. Kaminski,⁶⁵ M. H. Kelsey,⁶⁵ H. Kim,⁶⁵ P. Kim,⁶⁵ M. L. Kocian,⁶⁵ D. W. G. S. Leith,⁶⁵ S. Li,⁶⁵ B. Lindquist,⁶⁵ S. Luitz,⁶⁵ V. Luth,⁶⁵ H. L. Lynch,⁶⁵ D. B. MacFarlane,⁶⁵ H. Marsiske,⁶⁵ R. Messner,^{65,*} D. R. Muller,⁶⁵ H. Neal,⁶⁵ S. Nelson,⁶⁵ C. P. O'Grady,⁶⁵ I. Ofte,⁶⁵ M. Perl,⁶⁵ B. N. Ratcliff,⁶⁵ A. Roodman,⁶⁵ A. A. Salnikov,⁶⁵ R. H. Schindler,⁶⁵ J. Schwiening,⁶⁵ A. Snyder,⁶⁵ D. Su,⁶⁵ M. K. Sullivan,⁶⁵ K. Suzuki,⁶⁵ S. K. Swain,⁶⁵ J. M. Thompson,⁶⁵ J. Va'vra,⁶⁵ A. P. Wagner,⁶⁵ M. Weaver,⁶⁵ C. A. West,⁶⁵ W. J. Wisniewski,⁶⁵ M. Wittgen,⁶⁵ D. H. Wright,⁶⁵ H. W. Wulsin,⁶⁵ A. K. Yarritu,⁶⁵ C. C. Young,⁶⁵ V. Ziegler,⁶⁵ X. R. Chen,⁶⁶ H. Liu,⁶⁶ W. Park,⁶⁶ M. V. Purohit,⁶⁶ R. M. White,⁶⁶ J. R. Wilson,⁶⁶ M. Bellis,⁶⁷ P. R. Burchat,⁶⁷ A. J. Edwards,⁶⁷ T. S. Miyashita,⁶⁷ S. Ahmed,⁶⁸ M. S. Alam,⁶⁸ J. A. Ernst,⁶⁸ B. Pan,⁶⁸ M. A. Saeed,⁶⁸ S. B. Zain,⁶⁸ A. Soffer,⁶⁹ S. M. Spanier,⁷⁰ B. J. Wogslund,⁷⁰ R. Eckmann,⁷¹ J. L. Ritchie,⁷¹ A. M. Ruland,⁷¹ C. J. Schilling,⁷¹ R. F. Schwitters,⁷¹ B. C. Wray,⁷¹ B. W. Drummond,⁷² J. M. Izen,⁷² X. C. Lou,⁷² F. Bianchi,^{73a,73b} D. Gamba,^{73a,73b} M. Pelliccioni,^{73a,73b} M. Bomben,^{74a,74b} L. Bosisio,^{74a,74b} C. Cartaro,^{74a,74b} G. Della Ricca,^{74a,74b} L. Lanceri,^{74a,74b} L. Vitale,^{74a,74b} V. Azzolini,⁷⁵ N. Lopez-March,⁷⁵ F. Martinez-Vidal,⁷⁵ D. A. Milanes,⁷⁵ A. Oyanguren,⁷⁵ J. Albert,⁷⁶ Sw. Banerjee,⁷⁶ B. Bhuyan,⁷⁶ H. H. F. Choi,⁷⁶ K. Hamano,⁷⁶ G. J. King,⁷⁶ R. Kowalewski,⁷⁶ M. J. Lewczuk,⁷⁶ I. M. Nugent,⁷⁶ J. M. Roney,⁷⁶ R. J. Sobie,⁷⁶ T. J. Gershon,⁷⁷ P. F. Harrison,⁷⁷ J. Ilic,⁷⁷ T. E. Latham,⁷⁷ G. B. Mohanty,⁷⁷ E. M. T. Puccio,⁷⁷ H. R. Band,⁷⁸ X. Chen,⁷⁸ S. Dasu,⁷⁸ K. T. Flood,⁷⁸ Y. Pan,⁷⁸ R. Prepost,⁷⁸ C. O. Vucosalo,⁷⁸ and S. L. Wu⁷⁸

¹Laboratoire d'Annecy-le-Vieux de Physique des Particules (LAPP), Université de Savoie, CNRS/IN2P3, F-74941 Annecy-Le-Vieux, France

²Universitat de Barcelona, Facultat de Física, Departament ECM, E-08028 Barcelona, Spain

^{3a}INFN Sezione di Bari I-70126, Bari, Italy;

^{3b}Dipartimento di Fisica, Università di Bari, I-70126 Bari, Italy

⁴University of Bergen, Institute of Physics, N-5007 Bergen, Norway

⁵Lawrence Berkeley National Laboratory and University of California, Berkeley, California 94720, USA

⁶University of Birmingham, Birmingham, B15 2TT, United Kingdom

⁷Ruhr Universität Bochum, Institut für Experimentalphysik I, D-44780 Bochum, Germany

⁸University of British Columbia, Vancouver, British Columbia, Canada V6T 1Z1

⁹Brunel University, Uxbridge, Middlesex UB8 3PH, United Kingdom

¹⁰Budker Institute of Nuclear Physics, Novosibirsk 630090, Russia

¹¹University of California at Irvine, Irvine, California 92697, USA

¹²University of California at Riverside, Riverside, California 92521, USA

¹³University of California at San Diego, La Jolla, California 92093, USA

¹⁴University of California at Santa Barbara, Santa Barbara, California 93106, USA

¹⁵University of California at Santa Cruz, Institute for Particle Physics, Santa Cruz, California 95064, USA

¹⁶California Institute of Technology, Pasadena, California 91125, USA

¹⁷University of Cincinnati, Cincinnati, Ohio 45221, USA

¹⁸University of Colorado, Boulder, Colorado 80309, USA

¹⁹Colorado State University, Fort Collins, Colorado 80523, USA

²⁰Technische Universität Dortmund, Fakultät Physik, D-44221 Dortmund, Germany

²¹Technische Universität Dresden, Institut für Kern- und Teilchenphysik, D-01062 Dresden, Germany

²²Laboratoire Leprince-Ringuet, CNRS/IN2P3, Ecole Polytechnique, F-91128 Palaiseau, France

²³University of Edinburgh, Edinburgh EH9 3JZ, United Kingdom

^{24a}INFN Sezione di Ferrara, I-44100 Ferrara, Italy

^{24b}Dipartimento di Fisica, Università di Ferrara, I-44100 Ferrara, Italy

²⁵INFN Laboratori Nazionali di Frascati, I-00044 Frascati, Italy

^{26a}INFN Sezione di Genova, I-16146 Genova, Italy

^{26b}Dipartimento di Fisica, Università di Genova, I-16146 Genova, Italy

²⁷Harvard University, Cambridge, Massachusetts 02138, USA

²⁸Universität Heidelberg, Physikalisches Institut, Philosophenweg 12, D-69120 Heidelberg, Germany

²⁹Humboldt-Universität zu Berlin, Institut für Physik, Newtonstr. 15, D-12489 Berlin, Germany

³⁰Imperial College London, London, SW7 2AZ, United Kingdom

³¹University of Iowa, Iowa City, Iowa 52242, USA

³²Iowa State University, Ames, Iowa 50011-3160, USA

³³Johns Hopkins University, Baltimore, Maryland 21218, USA

³⁴Laboratoire de l'Accélérateur Linéaire, IN2P3/CNRS et Université Paris-Sud 11, Centre Scientifique d'Orsay, B. P. 34, F-91898 Orsay Cedex, France

³⁵Lawrence Livermore National Laboratory, Livermore, California 94550, USA

- ³⁶*University of Liverpool, Liverpool L69 7ZE, United Kingdom*
- ³⁷*Queen Mary, University of London, London, E1 4NS, United Kingdom*
- ³⁸*University of London, Royal Holloway and Bedford New College, Egham, Surrey TW20 0EX, United Kingdom*
- ³⁹*University of Louisville, Louisville, Kentucky 40292, USA*
- ⁴⁰*Johannes Gutenberg-Universität Mainz, Institut für Kernphysik, D-55099 Mainz, Germany*
- ⁴¹*University of Manchester, Manchester M13 9PL, United Kingdom*
- ⁴²*University of Maryland, College Park, Maryland 20742, USA*
- ⁴³*University of Massachusetts, Amherst, Massachusetts 01003, USA*
- ⁴⁴*Massachusetts Institute of Technology, Laboratory for Nuclear Science, Cambridge, Massachusetts 02139, USA*
- ⁴⁵*McGill University, Montréal, Québec, Canada H3A 2T8*
- ^{46a}*INFN Sezione di Milano, I-20133 Milano, Italy;*
- ^{46b}*Dipartimento di Fisica, Università di Milano, I-20133 Milano, Italy*
- ⁴⁷*University of Mississippi, University, Mississippi 38677, USA*
- ⁴⁸*Université de Montréal, Physique des Particules, Montréal, Québec, Canada H3C 3J7*
- ⁴⁹*Mount Holyoke College, South Hadley, Massachusetts 01075, USA*
- ^{50a}*INFN Sezione di Napoli, I-80126 Napoli, Italy*
- ^{50b}*Dipartimento di Scienze Fisiche, Università di Napoli Federico II, I-80126 Napoli, Italy*
- ⁵¹*NIKHEF, National Institute for Nuclear Physics and High Energy Physics, NL-1009 DB Amsterdam, The Netherlands*
- ⁵²*University of Notre Dame, Notre Dame, Indiana 46556, USA*
- ⁵³*Ohio State University, Columbus, Ohio 43210, USA*
- ⁵⁴*University of Oregon, Eugene, Oregon 97403, USA*
- ^{55a}*INFN Sezione di Padova, I-35131 Padova, Italy*
- ^{55b}*Dipartimento di Fisica, Università di Padova, I-35131 Padova, Italy*
- ⁵⁶*Laboratoire de Physique Nucléaire et de Hautes Energies, IN2P3/CNRS, Université Pierre et Marie Curie-Paris6, Université Denis Diderot-Paris7, F-75252 Paris, France*
- ⁵⁷*University of Pennsylvania, Philadelphia, Pennsylvania 19104, USA*
- ^{58a}*INFN Sezione di Perugia, I-06100 Perugia, Italy*
- ^{58b}*Dipartimento di Fisica, Università di Perugia, I-06100 Perugia, Italy*
- ^{59a}*INFN Sezione di Pisa, I-56127 Pisa, Italy*
- ^{59b}*Dipartimento di Fisica, Università di Pisa, I-56127 Pisa, Italy*
- ^{59c}*Scuola Normale Superiore di Pisa, I-56127 Pisa, Italy*
- ⁶⁰*Princeton University, Princeton, New Jersey 08544, USA*
- ^{61a}*INFN Sezione di Roma, I-00185 Roma, Italy*
- ^{61b}*Dipartimento di Fisica, Università di Roma La Sapienza, I-00185 Roma, Italy*
- ⁶²*Universität Rostock, D-18051 Rostock, Germany*
- ⁶³*Rutherford Appleton Laboratory, Chilton, Didcot, Oxon, OX11 0QX, United Kingdom*
- ⁶⁴*CEA, Irfu, SPP, Centre de Saclay, F-91191 Gif-sur-Yvette, France*
- ⁶⁵*SLAC National Accelerator Laboratory, Stanford, California 94309 USA*
- ⁶⁶*University of South Carolina, Columbia, South Carolina 29208, USA*
- ⁶⁷*Stanford University, Stanford, California 94305-4060, USA*
- ⁶⁸*State University of New York, Albany, New York 12222, USA*
- ⁶⁹*Tel Aviv University, School of Physics and Astronomy, Tel Aviv, 69978, Israel*
- ⁷⁰*University of Tennessee, Knoxville, Tennessee 37996, USA*
- ⁷¹*University of Texas at Austin, Austin, Texas 78712, USA*
- ⁷²*University of Texas at Dallas, Richardson, Texas 75083, USA*
- ^{73a}*INFN Sezione di Torino, I-10125 Torino, Italy*
- ^{73b}*Dipartimento di Fisica Sperimentale, Università di Torino, I-10125 Torino, Italy*
- ^{74a}*INFN Sezione di Trieste, I-34127 Trieste, Italy*
- ^{74b}*Dipartimento di Fisica, Università di Trieste, I-34127 Trieste, Italy*
- ⁷⁵*IFIC, Universitat de Valencia-CSIC, E-46071 Valencia, Spain*
- ⁷⁶*University of Victoria, Victoria, British Columbia, Canada V8W 3P6*

*Deceased

†Now at Temple University, Philadelphia, PA 19122, USA.

‡Also with Università di Perugia, Dipartimento di Fisica, Perugia, Italy.

§Also with Università di Roma La Sapienza, I-00185 Roma, Italy.

||Now at University of South Alabama, Mobile, AL 36688, USA.

¶Also with Laboratoire de Physique Nucléaire et de Hautes Energies, IN2P3/CNRS, Université Pierre et Marie Curie-Paris6, Université Denis Diderot-Paris7, F-75252 Paris, France.

**Also with Università di Sassari, Sassari, Italy.

⁷⁷*Department of Physics, University of Warwick, Coventry CV4 7AL, United Kingdom*⁷⁸*University of Wisconsin, Madison, Wisconsin 53706, USA*

(Received 18 September 2009; published 20 November 2009)

We present the result from a precision measurement of the mass of the τ lepton, M_τ , based on 423 fb⁻¹ of data recorded at the $\Upsilon(4S)$ resonance with the *BABAR* detector. Using a pseudomass endpoint method, we determine the mass to be $1776.68 \pm 0.12(\text{stat}) \pm 0.41(\text{syst})$ MeV. We also measure the mass difference between the τ^+ and τ^- , and obtain $(M_{\tau^+} - M_{\tau^-})/M_{\text{AVG}}^\tau = (-3.4 \pm 1.3(\text{stat}) \pm 0.3(\text{syst})) \times 10^{-4}$, where M_{AVG}^τ is the average value of M_{τ^+} and M_{τ^-} .

DOI: 10.1103/PhysRevD.80.092005

PACS numbers: 13.25.Hw, 11.30.Er, 12.15.Hh

I. INTRODUCTION

Masses of quarks and leptons are fundamental parameters of the standard model. They cannot be determined by the theory and must be measured. A precise measurement of the mass of the τ lepton is important for testing lepton universality [1] and for calculating branching fractions that depend on the τ mass [2]. Uncertainties in the τ mass have important consequences on the accuracy of the calculated leptonic-decay rate of the τ , proportional to M_τ^5 [3].

CPT invariance is a fundamental symmetry of any local field theory, including the standard model. Any evidence of *CPT* violation would be evidence of local Lorentz violation and a sign of physics beyond the standard model [4–7]. The most common tests of *CPT* invariance are measurements of the differences of the masses and lifetimes of particles and their antiparticles. The most precise test of *CPT* invariance is from the measured limits of the mass difference of neutral kaons, $|M_{K^0} - M_{\bar{K}^0}|/M_{\text{AVG}}^K < 8 \times 10^{-19}$ [8] at 90% confidence level (C.L.), where M_{AVG}^K is the average value of M_{K^0} and $M_{\bar{K}^0}$.

At the $\Upsilon(4S)$ resonance, the cross section for $e^+e^- \rightarrow \tau^+\tau^-$ is 0.919 ± 0.003 nb [9], resulting in a very large data sample, comparable to the number of $b\bar{b}$ events produced. With this data sample we can perform a pseudomass-endpoint measurement, first used by the ARGUS Collaboration [10] and recently by the Belle Collaboration [11], to measure the mass of the τ lepton. Unlike the production-threshold method used by the BES [1] and KEDR [12] experiments, this pseudomass method has the advantage of measuring the mass of the τ^+ and τ^- separately, which allows us to test the *CPT* theorem by measuring their mass difference. This measurement was first performed by the OPAL Collaboration [13], and the current limit is $|M_{\tau^+} - M_{\tau^-}|/M_{\text{AVG}}^\tau < 2.8 \times 10^{-4}$ [8] at 90% C.L.: the Particle Data Group (PDG) average value of the τ mass is $M_{\text{AVG}}^\tau = 1776.84 \pm 0.17$ MeV [8]. Tables I and II summarize the most recent measurements of M_τ and the measured upper limits of $|M_{\tau^+} - M_{\tau^-}|/M_{\text{AVG}}^\tau$.

The pseudomass is defined in terms of the mass, energy, and momenta of the τ decay products. For hadronic decays of the τ^- ($\tau^- \rightarrow h^- \nu_\tau$ and its charge conjugate), the τ mass, M_τ , is given by

$$M_\tau = \sqrt{M_h^2 + 2(\sqrt{s}/2 - E_h^*)(E_h^* - P_h^* \cos\theta^*)}, \quad (1)$$

where θ^* is the angle between the hadronic system and the ν_τ and M_h , E_h , and P_h are the mass, energy, and magnitude of the three-momentum of the hadronic system h , respectively. The * indicates quantities in the e^+e^- center-of-mass (CM) frame. In the CM frame, the energy of the τ is given by $E_\tau^* = \sqrt{s}/2$, where $\sqrt{s} = 10.58$ GeV. This relation ignores initial state radiation (ISR) from the e^+e^- beams and final state radiation (FSR) from the τ leptons. We also assume $M_{\nu_\tau} = 0$. Since the neutrino is undetected, we cannot measure the angle θ^* , thus we define the pseudomass M_p by setting $\theta^* = 0$

$$M_p \equiv \sqrt{M_h^2 + 2(\sqrt{s}/2 - E_h^*)(E_h^* - P_h^*)} \leq M_\tau. \quad (2)$$

Figure 1 shows the pseudomass distribution after applying all of the selection criteria (Sec. III) and the sharp kinematic cutoff at $M_p = M_\tau$. The smearing of the endpoint and large tail in the distribution is caused by ISR and FSR and detector resolution. The τ mass is measured by determining the position of the endpoint. We choose to use the decay mode $\tau^- \rightarrow \pi^- \pi^+ \pi^- \nu_\tau$ and its charge conjugate, since it has a relatively large branching ratio, $\mathcal{B}(\tau^- \rightarrow \pi^- \pi^+ \pi^- \nu_\tau) = (8.99 \pm 0.06)\%$ [8], has a high signal purity, and has large statistics in the endpoint region due to the large central value and width of the mass distribution of the 3π system.

TABLE I. Recent τ mass measurements.

Experiment	M_τ (MeV)
BES [1]	$1776.96^{+0.18+0.25}_{-0.21-0.17}$
KEDR [12]	$1776.81^{+0.25}_{-0.23} \pm 0.15$
Belle [11]	$1776.61 \pm 0.13 \pm 0.35$

TABLE II. Measured upper limits of the τ^+ and τ^- mass difference at 90% C.L.

Experiment	$ M_{\tau^+} - M_{\tau^-} /M_{\text{AVG}}^\tau$
OPAL [13]	$< 3.0 \times 10^{-3}$
Belle [11]	$< 2.8 \times 10^{-4}$

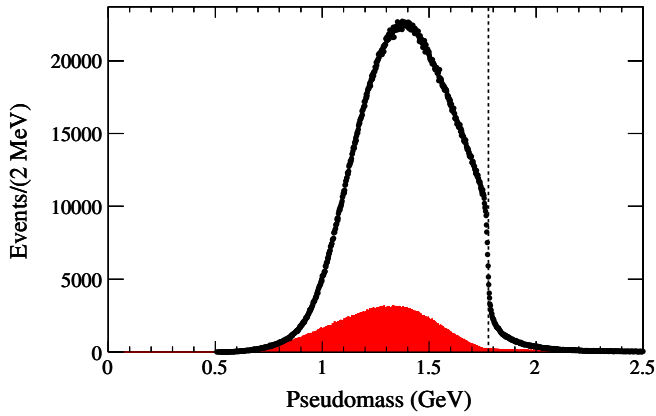


FIG. 1 (color online). Pseudomass distribution. The points are data, the solid area is the background estimated from MC, and the dashed vertical line represents the PDG average value of the τ mass [8]. Note the sharp edge of the distribution at the τ mass.

II. THE *BABAR* DETECTOR AND DATASET

The data used in this analysis were collected with the *BABAR* detector at the PEP-II asymmetric-energy e^+e^- storage rings operating at the SLAC National Accelerator Laboratory. We use 423 fb^{-1} of data collected at the $Y(4S)$ resonance corresponding to over 388 million $\tau^+\tau^-$ pairs. For the control samples of inclusive $K_S^0 \rightarrow \pi^+\pi^-$, $D^+ \rightarrow K^-\pi^+\pi^+$, $D^+ \rightarrow \phi\pi^+$, $D_s^+ \rightarrow \phi\pi^+$, and their charge conjugates used for systematic studies, we use about 100, 100, 423, and 423 fb^{-1} of data, respectively. The background Monte Carlo (MC) samples used for this analysis comprise of generic $e^+e^- \rightarrow Y(4S) \rightarrow B\bar{B}$ events simulated with the *EvtGen* generator [14], and $e^+e^- \rightarrow q\bar{q}$ ($q = u, d, s, c$) continuum events simulated with the *JETSET7.4* generator [15]. For simulation of τ pair events we use the MC generators *KK2F* [16] and *TAUOLA* [17], and use *PHOTOS* [18] to incorporate FSR. For the extraction of the τ mass, we generate signal samples with three different τ masses ($M_\tau = 1774, 1777, \text{ and } 1780 \text{ MeV}$), each comparable in event totals to the data sample. The *BABAR* detector and its response to particle interactions are modeled using the *GEANT4* simulation package [19].

The *BABAR* detector is described in detail elsewhere [20]. The momenta of the charged particles are measured with a combination of a five-layer silicon vertex tracker (SVT) and a 40-layer drift chamber (DCH) in a 1.5 T solenoidal magnetic field. A detector of internally reflected Cherenkov radiation is used for charged particle identification. Kaons and protons are identified with likelihood ratios calculated from dE/dx measurements in the SVT and DCH, and from the observed pattern of Cherenkov light in the detector of internally reflected Cherenkov radiation. A finely segmented CsI(Tl) electromagnetic calorimeter is used to detect and measure photons and neutral hadrons, and to identify electrons. The instrumented flux return contains resistive plate chambers and

limited streamer tubes [21] to identify muons and long-lived neutral hadrons.

The most critical aspect of this analysis is the reconstruction of the charged particle momenta. Tracks are selected using the information collected by the SVT and DCH using a track finding algorithm: they are then refit using a Kalman filter method to refine the track parameters [22]. This algorithm corrects for the energy loss and multiple scattering of the charged particles interacting with the detector material and for any inhomogeneities of the magnetic field according to a detailed model of the tracking environment. Since the energy loss depends on particle velocity, the Kalman filter is performed separately for five mass hypotheses: electron, muon, pion, kaon, and proton. The main components of the detector to be modeled for charged particle tracks originating from the vicinity of the interaction point are the 1.4 mm thick beryllium-beam pipe and 1.5 mm of cooling water at a radius of 2.5 cm, five layers of 300 μm thick silicon at radii of 3.3 cm to 15 cm, a 2 mm thick carbon-fiber tube at 22 cm that is used to support the SVT, and a 1 mm thick beryllium tube at 24 cm that makes up the inner wall of the DCH. Detailed knowledge of the material in the tracking volume and the magnetic field is crucial to accurate momentum reconstruction [23]. This information is based on detailed information from engineering drawings and measurements taken both before and after the commissioning of the detector.

III. ANALYSIS METHOD

For our event selection, we require exactly four tracks in the event, none of which is identified as a charged kaon or proton. We veto events with $K_S^0 \rightarrow \pi^+\pi^-$ candidates with an invariant mass within $\pm 25 \text{ MeV}$ of the nominal K_S^0 mass [8] and $\pi^0 \rightarrow \gamma\gamma$ candidates constructed with photons with CM energy greater than 30 MeV and an invariant mass in the range $100 \text{ MeV} \leq M_{\gamma\gamma} \leq 160 \text{ MeV}$. We require the total charge of the event to be zero. We divide the event into two hemispheres defined by the plane perpendicular to the event-thrust axis in the CM frame, which is calculated using all tracks and photon candidates. One hemisphere of the event, the tag side, must have a single track identified as either an electron or muon, and in the opposite hemisphere, the signal side, we require three charged tracks, none identified as a lepton. In addition to the π^0 veto, we require the number of photons with CM energy greater than 50 MeV on the signal side to be less than 5 and the total photon energy on the signal side to be less than 300 MeV to further reduce sources of background with one or more neutral pions.

To reduce background events from two-photon processes, we apply six additional selection criteria. We require the total reconstructed energy of the event to be within the range $2.5 \text{ GeV} \leq E_{\text{tot}}^* \leq 9.0 \text{ GeV}$ and the thrust magnitude to be greater than 0.85, where these quantities

are calculated with all tracks and neutrals with CM energy greater than 50 MeV. We require the tag lepton to have an energy less than 4.8 GeV, the energy of the three-pion system on the signal side to be $1.0 \text{ GeV} \leq E_{3\pi}^* \leq 5.2 \text{ GeV}$, and the reconstructed mass of the 3π system to be greater than 0.5 GeV. We also require the polar angle of the missing momentum to be in the range $-0.95 \leq \cos\theta_{\text{miss}}^* \leq 0.92$.

We define our fit region to be $1.68 \leq M_p \leq 1.86 \text{ GeV}$. After all requirements, our signal efficiency is 2.0% and the purity of our sample is 96%. Our largest background is $\tau^- \rightarrow 2\pi^- \pi^+ \pi^0 \nu_\tau$, where the π^0 is not reconstructed. The total number of events in the data is 3.42×10^5 , 3.40×10^5 , 3.52×10^5 , and 3.29×10^5 for the τ^+ , τ^- , e tag, and μ tag, respectively.

We use three MC samples with different τ masses (1774, 1777, and 1780 MeV) to empirically determine the relation between the pseudomass endpoint and the τ mass, accounting for the smearing due to resolution and ISR or FSR effects.

To determine the endpoint from the pseudomass distribution, we perform an unbinned-maximum-likelihood fit to the data using an empirical function [11] of the form

$$F(x) = (p_3 + p_4 x) \tan^{-1} \left(\frac{p_1 - x}{p_2} \right) + p_5 + p_6 x, \quad (3)$$

where x is the pseudomass, and the p_i are free parameters of the fit. Only the position of the endpoint, p_1 , is important in determining the τ mass, as the shape of the distribution does not affect the edge position since the correlation between p_1 and the other parameters is small.

Figure 2 shows the pseudomass distributions from the three MC samples, with the shift in the edge clearly visible. We fit each one of the MC distributions, and Fig. 3 shows the fit results for p_1 versus the generated τ mass. In the absence of ISR or FSR effects and with perfect detector

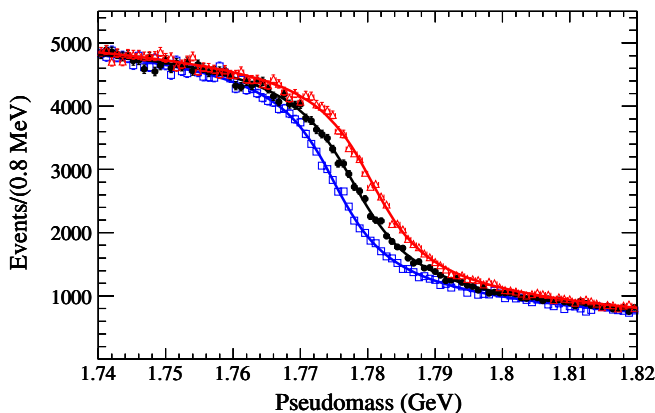


FIG. 2 (color online). Pseudomass endpoint distributions from the three MC samples. The open squares, dots, and open triangles are for generated τ mass values of 1774, 1777, and 1780 MeV, respectively, and the curves are the results of the fits to the samples.

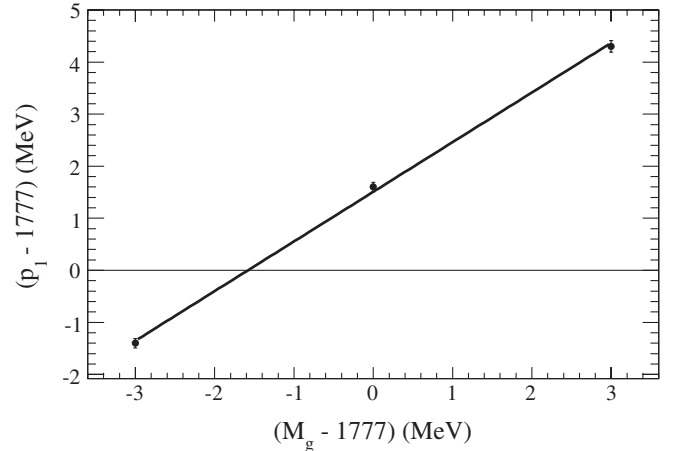


FIG. 3. The fitted value of p_1 as a function of M_g , the value of M_τ in the simulation. These fit results are used in the determination of M_τ from the endpoint fit to the data.

resolution we would expect the relation between the p_1 fit result and generated τ mass to be linear with a slope of unity and $y - \text{intercept} = 0$. With the inclusion of the ISR and FSR effects and detector resolution, we expect the relationship to still be linear with a slope of unity but to have a nonzero offset. We fit the results to a linear function, $(p_1 - 1777 \text{ MeV}) = a_1(M_g - 1777 \text{ MeV}) + a_0$, where M_g is the generated τ mass, and a_0 and a_1 are free parameters of the fit. The results of the straightline fit are $a_1 = 0.96 \pm 0.02$ and $a_0 = 1.49 \pm 0.05 \text{ MeV}$. We use the results from the straightline fit to determine the value of the τ mass from the endpoint fit of the data.

To determine the mass difference, we split our data sample into two sets based on the total charge of the three-pion signal tracks. We use the combined fit results for a_1 and a_0 to determine the mass of τ^+ and τ^- . As a cross check, we split our MC in the same way and repeat the procedure described above for each sample. We find the individual fit results for a_1 and a_0 to be within one sigma of the combined fit results.

IV. TRACK MOMENTUM RECONSTRUCTION

A previous analysis [23] of *BABAR* data has revealed that the track reconstruction procedure leads to systematic underestimation of the individual track momentum. This effect is not observed for MC simulation. There are two potential sources of bias in the track momentum measurement: errors in the detector model which could lead to a momentum-dependent bias, and incorrect modeling of the magnetic field strength in the tracking volume, which leads to a bias independent of momentum. We use a $K_S^0 \rightarrow \pi^+ \pi^-$ control sample to investigate this bias and determine a correction. The K_S^0 daughter pions have a momentum distribution similar to the pions in our signal sample, and the long flight length of the K_S^0 is ideal for studying the

energy loss correction used by the reconstruction algorithm. The K_S^0 candidates are reconstructed from two oppositely charged tracks that have an invariant mass within 25 MeV of the nominal K_S^0 mass value [8]. This sample comprises 2.96×10^6 K_S^0 candidates. We determine the K_S^0 mass by performing a maximum-likelihood fit to the data using a function which is a sum of two Gaussian distribution functions with a common mean and different widths, and a second order polynomial to describe the background. The background is relatively flat and does not affect the measurement of the K_S^0 mass. We increase the amount of SVT material, the strength of the solenoid field, and the strength of the field due to the magnetization of the beam-line dipole magnets inside the detector model to correct the reconstructed track momenta. The increases of the material in the SVT and the strength of the solenoid field are chosen to improve the agreement of the reconstructed K_S^0 mass with the world average value [8]. These increases are larger than the estimated uncertainties. In the following we detail the procedure to derive these corrections.

A. Energy loss

Track momenta are corrected for energy loss by the Kalman filter procedure. The amount of energy a particle loses due to material interactions depends on the nature and amount of material traversed and the type and momentum of the particle. Thus, any error in the estimated energy loss will vary with the amount of material the track traverses and the laboratory (lab) momentum of the track.

There is clear evidence that track momenta are underestimated for our nominal reconstruction procedure, as shown in Fig. 4. The K_S^0 sample, as a function of the decay-vertex radius, ranges in purity from 7% to 91%, with the lowest purity arising from the interaction region, when the candidates have very short flight distances. The larger the radial distance of the K_S^0 decay vertex, the less material the charged pions traverse, decreasing the size of the energy-loss correction. The largest deviation is seen for those events where the K_S^0 vertex is closest to the interaction region. This dependence of the reconstructed K_S^0 mass on the amount of material traversed by the pions demonstrates that the energy-loss correction is underestimated. Figure 4 also shows the K_S^0 mass as a function of the K_S^0 lab momentum: the purity of the sample ranges from 14% to 83% with increasing momenta. We see that lower momenta K_S^0 particles have masses further from the expected K_S^0 mass than high momenta ones, since the energy-loss corrections are greater for the lower momenta particles, because the K_S^0 decay-vertex radius and K_S^0 momentum are correlated.

We study two possible corrections to the energy-loss underestimation: increasing the amount of SVT material by 20% and increasing the amount of material in the entire-tracking volume by 10% [23]. For each correction, we increase the density of the corresponding detector material

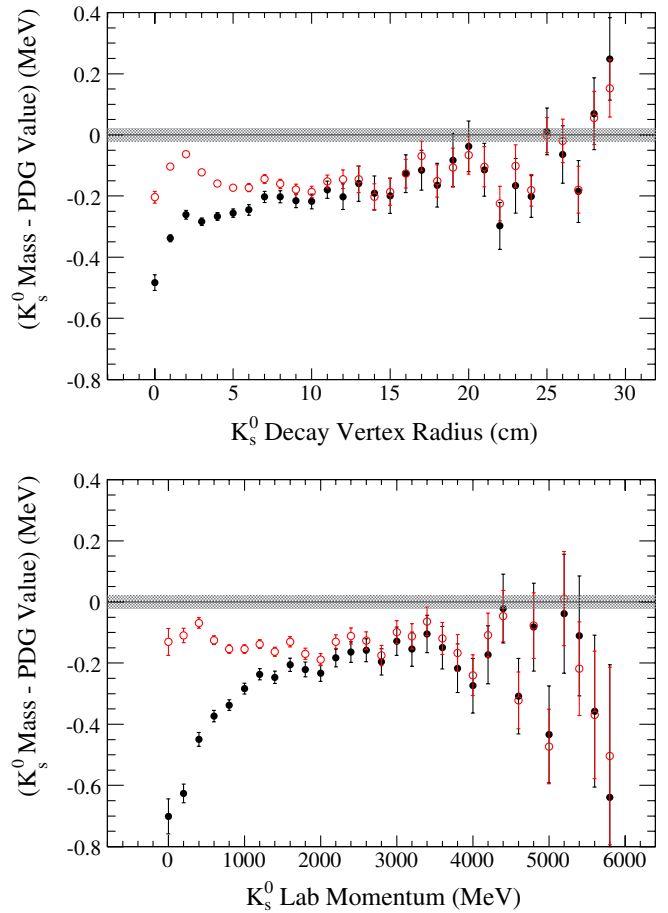


FIG. 4 (color online). Fitted K_S^0 mass vs decay-vertex radius (top panel) and K_S^0 lab momentum (bottom panel). On the vertical axis, the PDG average value of the K_S^0 mass [8] has been subtracted from the fitted value. The points show the normally reconstructed data events, the open circles show the data reconstructed with 20% more SVT material, and the shaded region is the error on the nominal K_S^0 mass [8]. The dependence of the K_S^0 mass on the decay-vertex radius and momentum is due to the underestimation of the energy loss by the reconstruction procedure.

by the indicated amount and repeat the Kalman filter procedure again. Figures. 4 and 5 show the resulting K_S^0 mass variations after these corrections. In the case where the entire-tracking-volume is increased, we observe that the K_S^0 mass variation with the decay-vertex radius is flat, but the K_S^0 mass is over-corrected at lower momenta. A smaller correction of the entire tracking material could be used to flatten the K_S^0 mass variation with the momentum, but then the K_S^0 mass variation with the decay-vertex radius would no longer be flat. Therefore, we do not use the increase of the entire tracking material in our correction. In the case where the SVT material is increased, we observe that the K_S^0 mass variation with decay-vertex radius and momentum is substantially reduced and flat. This reduction and flattening of the dependence of the recon-

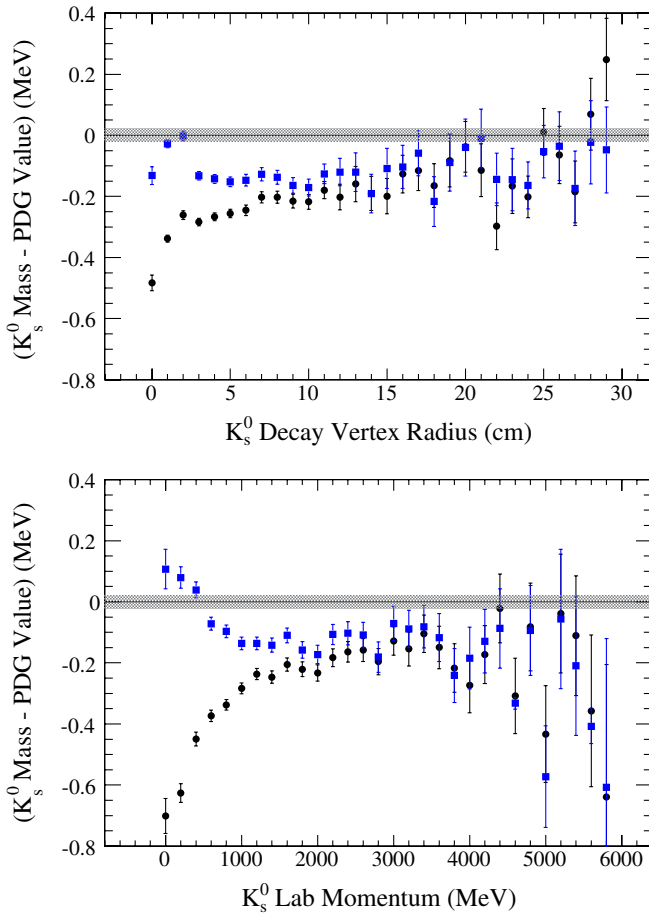


FIG. 5 (color online). Fitted K_S^0 mass vs decay-vertex radius (top panel) and lab momentum (bottom panel). On the vertical axis, the PDG average value of the K_S^0 mass [8] has been subtracted from the fitted value. The points show the normally reconstructed data events, the squares show the data reconstructed with 10% more material in the tracking volume, and the shaded region is the error on the nominal K_S^0 mass [8].

structed K_S^0 mass on the vertex position and momentum is our motivation for applying this correction to our material model. The estimated uncertainty in the SVT material is about 4.5% as determined from detailed analyses of the composition of the SVT and its electronics: the 20% increase significantly exceeds this estimated uncertainty. We apply it as a simplified method to account for this and all other uncertainties in the energy loss estimation. The uncertainty in this simple correction accounts for the largest uncertainty in the τ mass measurement.

B. Magnetic field

After the SVT energy-loss correction, we find that the K_S^0 mass is still underestimated. In order to further correct the K_S^0 mass, we consider two possible sources of error: uncertainty in the 1.5 T solenoidal magnetic field that runs parallel to the beam axis and the perturbation to this field due to the magnetization of the magnetic materials com-

prising the beamline dipole magnets (BDM) due to the solenoid field.

The BDM are permanent magnets, made of samarium-cobalt, the closest of which is located 20 cm away from the interaction region. The fringe fields from these magnets in the interaction region are small and have been well measured; however the magnetic field due to the magnetization of these magnets by the solenoid field is not well known. The permeability of the BDM material was not measured before the commissioning of the detector, and subsequently variations in the susceptibility of $\pm 20\%$ with respect to the average value ($+0.14$) have been found within the individual small blocks used to construct the BDM. The field in the tracking volume due to the magnetization was estimated from measurements made at two points near the BDM, using Hall and nuclear magnetic resonance probes, followed by finite element calculations that depend on the permeability of the magnets. In 2002, the probes were moved and the field was remeasured at two new points. At one point, there was good agreement with expectation, but at the other point the overall value of the field strength was 0.4% higher than expected. We increase the field due to the magnetization of the BDM by 20% to account for the variation of the measured permeability of these magnets and the observed discrepancy between the measured and estimated fields, in order to improve the agreement of our reconstructed K_S^0 mass with the world average value [8]. Figure 6 shows the effect of the increase on the K_S^0 mass as a function of the K_S^0 momentum measured in the lab frame.

The solenoid field was very accurately measured with an uncertainty of 0.2 mT prior to the installation of the BDM

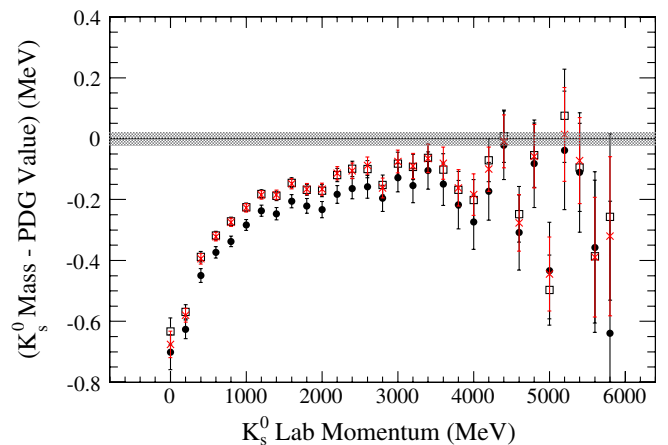


FIG. 6 (color online). Fitted K_S^0 mass vs lab momentum. On the vertical axis, the PDG average value of the K_S^0 mass [8] has been subtracted from the fitted value. The points show the normally reconstructed data, the open squares show the data reconstructed with the solenoid field increased by 0.02%, the crosses show the data reconstructed with magnetization field increased by 20%, and the shaded region is the error on the nominal K_S^0 mass [8].

TABLE III. Shifts in the measured mean value of the K_S^0 mass when each track reconstruction correction is applied separately and comparison with the nominal value [8].

Fit	$M_{K_S^0}$ (MeV)	Mass Shift (MeV)
Default Reconstruction	497.323	-
SVT Material +20.0%	497.477	+0.154
Solenoid Field +0.02%	497.383	+0.060
BDM Field +20.0%	497.382	+0.059
Fully Corrected	497.596 ± 0.006	-
PDG Average	497.614 ± 0.024	-

during the commissioning of the detector. To further correct the K_S^0 mass, we increase the solenoid field by 0.02%, and then refit the tracks. Figure 6 shows the effect of this increase. This increase is larger than the measured uncertainty in the solenoid field, but it further improves the agreement of our reconstructed K_S^0 mass with the world average value [8]. Table III shows that this increase, in conjunction with the increases of the SVT material and the BDM magnetization field, shifts the K_S^0 mass so that it is consistent with the world average value [8].

C. Momentum reconstruction correction

We study the overall corrections described above for K_S^0 and D^\pm decays. These corrections affect the reconstructed masses in different ways. Although the size of the correction varies depending on the decay kinematics, decay mode, and the mass of the particle being reconstructed, the masses of our test samples are consistent with the world averages after the corrections are applied. To determine the size of a correction, we increase the amount of SVT material, the field due to the BDM, and the solenoid field strength in three separate simulations. For each of these simulations we refit each pion track using the Kalman fit procedure described above, and recalculate the reconstructed mass. The overall mass correction is taken as the sum of the three individual mass shifts, and the corrected mass is determined by adding the correction to the mass determined with the normal reconstruction. Figure 7 shows the corrected K_S^0 mass as a function of the K_S^0 decay-vertex radius and momentum in the lab frame. This method improves the agreement of our measured K_S^0 mass with the world average. Table III shows the individual corrections as well as the overall correction for the K_S^0 mass.

We also apply this method to the decay $D^+ \rightarrow K^- \pi^+ \pi^+$ and its charge conjugate. We perform a vertex fit to the three tracks and require the vertex probability to be greater than 0.1%. We also require the mass of the candidate to be in the range $1.84 \text{ GeV} \leq M_D \leq 1.90 \text{ GeV}$. To determine the mass of the D meson, we perform a maximum-likelihood fit to the $K\pi\pi$ mass distribution using a function which is a sum of two Gaussian distribution functions with a common mean and different

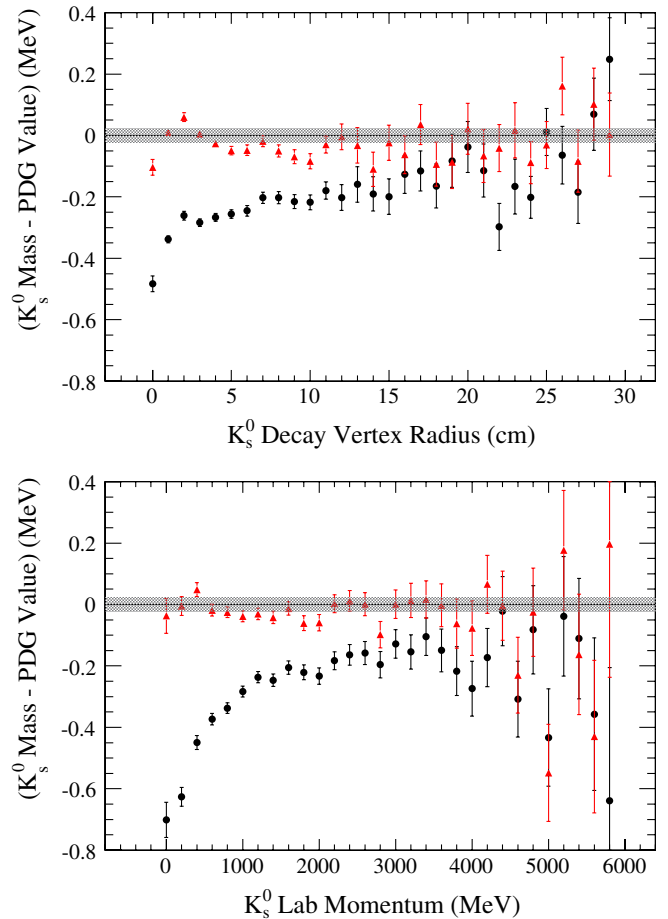


FIG. 7 (color online). Fitted K_S^0 mass vs decay-vertex radius (top panel) and lab momentum (bottom panel). On the vertical axis, the PDG average value of the K_S^0 mass [8] has been subtracted from the fitted value. The points show the normally reconstructed data, the triangles show the data after the correction from the increased material and magnetic-field strengths has been applied, and the shaded region is the error on the nominal K_S^0 mass [8].

widths and a second order polynomial to describe the background. Table IV summarizes the result of the fits with the normal reconstruction and modified detector model. We find that the measured mass using the normal

TABLE IV. Shifts in the measured mean value of the D^\pm mass when each track reconstruction correction is applied separately and comparison with the nominal value [8].

Fit	M_{D^\pm} (MeV)	Mass Shift (MeV)
Default Reconstruction	1868.70	-
SVT Material +20.0%	1869.17	+0.47
Solenoid Field +0.02%	1869.00	+0.30
BDM Field +20.0%	1869.00	+0.30
Fully Corrected	1869.77 ± 0.04	-
PDG Average	1869.62 ± 0.20	-

TABLE V. Observed shifts for M_τ in the data due to each correction applied to the reconstructed track momenta separately and total correction.

Detector Parameter	M_τ Shift (MeV)
SVT Material +20.0%	+0.31
Solenoid Field +0.02%	+0.11
BDM Field +20.0%	+0.21
Correction	+0.63

reconstruction differs by -0.92 MeV relative to the world average value of 1869.62 ± 0.20 MeV [8]; after applying the correction, the difference is reduced to $+0.15$ MeV, in very good agreement within the current uncertainties.

We apply this method to the events in the sample of $\tau^- \rightarrow \pi^- \pi^+ \pi^- \nu_\tau$ and its charge conjugate and obtain a correction of $+0.63$ MeV for the τ mass. Table V shows the individual shifts on the τ mass.

D. Charge asymmetry

The π^+ and π^- tracking efficiencies differ because of different cross sections for interactions of low-momentum π^+ and π^- with the detector material [8]. This could cause differences between the reconstruction efficiencies for $\tau^+ \rightarrow \pi^- \pi^+ \pi^+ \bar{\nu}_\tau$ and $\tau^- \rightarrow \pi^- \pi^+ \pi^- \nu_\tau$. A difference in the reconstruction efficiency for the τ^+ and τ^- might introduce a dependence of the reconstructed τ mass on the τ momentum and thus might result in an artificial mass difference.

To estimate any charge asymmetry in the track reconstruction procedure, we measure the mass difference in several control samples: $D^+ \rightarrow K^- \pi^+ \pi^+$, $D^+ \rightarrow \phi \pi^+$, $D_s^+ \rightarrow \phi \pi^+$, and their charge conjugates. The momentum spectra of the daughter pions in the τ signal sample are similar to the spectra in the three control samples. The selection criteria for the $D^+ \rightarrow K^- \pi^+ \pi^+$ and charge conjugate modes are described in Sec. IV C. The ϕ candidates are reconstructed from two oppositely charged kaons, and the reconstructed mass of the ϕ candidate is required to be within ± 12 MeV of the nominal value [8]. To reconstruct a D or D_s candidate, the two kaon tracks from the ϕ candidate are combined with a pion track, and the three tracks are required to have a vertex probability greater than 0.1%. The D and D_s candidates are required to have a CM momentum greater than 2.4 GeV to further reduce backgrounds. The D and D_s candidates are required to have an invariant mass within the range $1.85 \text{ GeV} \leq M_D \leq 1.90 \text{ GeV}$ and $1.95 \text{ GeV} \leq M_{D_s} \leq 1.99 \text{ GeV}$. For the three samples, respectively, the total numbers of events are 4.5×10^6 , 1.7×10^6 , and 2.2×10^6 , and the purities are 33%, 90%, and 87%. To determine the masses, we perform a maximum-likelihood fit to each three-particle invariant-mass distribution, again using a sum of two Gaussian distribution functions with a common mean and

TABLE VI. ΔM for the D^\pm and D_s^\pm meson control samples used to study the possible charge asymmetry.

Sample	Mass Difference (MeV)
$D^+ \rightarrow K^- \pi^+ \pi^+$	-0.04 ± 0.03
$D^+ \rightarrow \phi \pi^+$	$+0.06 \pm 0.04$
$D_s^+ \rightarrow \phi \pi^+$	$+0.10 \pm 0.05$

different widths and a second order polynomial background function. Table VI shows the observed mass difference, $\Delta M \equiv M_{X^+} - M_{X^-}$, for each of the three decay modes, where X is the particle whose mass is measured. The results are consistent with zero difference. Thus, we do not make any correction and use these results to determine the systematic uncertainty in $M_{\tau^+} - M_{\tau^-}$ due to the possible residual uncertainty in tracking. As a cross check, we perform the study on a sample of $D^+ \rightarrow \phi \pi^+$, $D_s^+ \rightarrow \phi \pi^+$, and charge conjugates where we do not constrain the momentum of the D and D_s . We find the mass difference of these samples is consistent with the results using the samples that have a D and D_s momentum constraint.

V. RESULTS

Figure 8 shows the pseudomass distribution of the combined τ^+ and τ^- samples compared to the fitted distribution. The fitted value of the endpoint position is $p_1 = 1777.58 \pm 0.12$ MeV. Using the MC results for a_0 and a_1 and applying the reconstruction procedure corrections described in Sec. IV C, we obtain $M_\tau = 1776.68 \pm 0.12$ MeV, where the error is statistical only.

Figure 9 shows the resulting pseudomass distribution from subtracting the τ^- distribution from the τ^+ distribution. We measure $p_1(\tau^+)$ to be 1777.29 ± 0.16 MeV and $p_1(\tau^-) = 1777.88 \pm 0.17$ MeV. Applying the above pro-

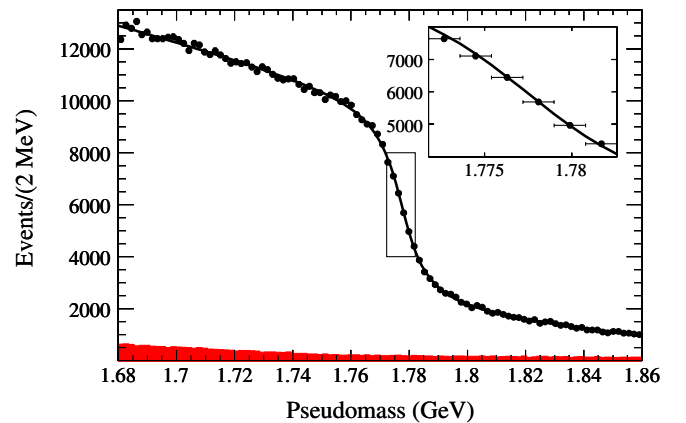


FIG. 8 (color online). Combined τ^+ and τ^- pseudomass endpoint distribution. The points show the data, the curve is the fit to the data, and the solid area is the background. The inset is an enlargement of the boxed region around the edge position showing the fit quality where p_1 is most sensitive.

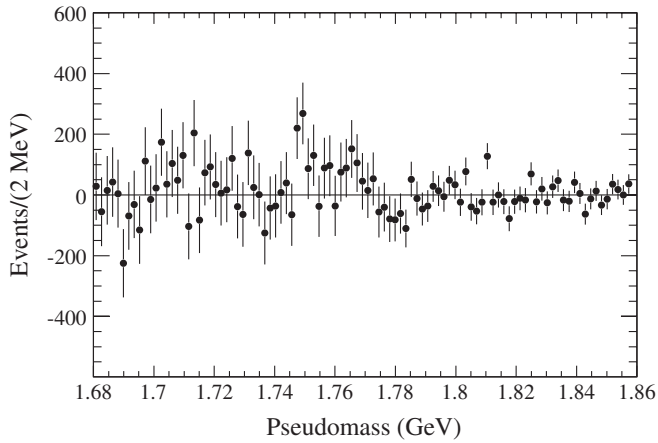


FIG. 9. Resulting pseudomass distribution from subtracting the τ^- distribution from the τ^+ distribution.

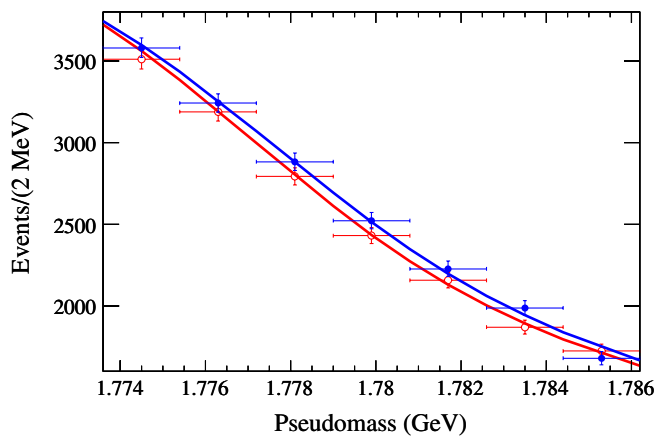


FIG. 10 (color online). Pseudomass distributions for the τ^+ and τ^- in the region around the pseudomass threshold region. The open circles and solid points show the τ^+ and τ^- distributions, respectively. The curves show the results of the fits to the data.

cedure, we find $M_{\tau^+} = 1776.38 \pm 0.16$ MeV and $M_{\tau^-} = 1776.99 \pm 0.17$ MeV, where the errors are statistical only. Thus, $M_{\tau^+} - M_{\tau^-} = -0.61 \pm 0.23(\text{stat})$ MeV. Figure 10 shows the pseudomass threshold region, where the τ^- distribution is clearly shifted to a higher mass relative to the τ^+ distribution.

VI. SYSTEMATIC STUDIES

Table VII summarizes the estimated systematic uncertainties in M_τ .

The largest source of error in the τ mass measurement arises from the momentum-reconstruction uncertainty. The increases in the SVT material and magnetic-field strengths are applied to obtain a better agreement of the reconstructed K_S^0 mass with the nominal K_S^0 mass [8], but the actual cause of the discrepancy is still unknown. The effect of the induced magnetization of the BDM on the magnetic

TABLE VII. Systematic uncertainties in M_τ .

Source	Uncertainty (MeV)
Momentum Reconstruction	0.39
CM Energy	0.09
MC Modeling	0.05
MC Statistics	0.05
Fit Range	0.05
Parametrization	0.03
Total	0.41

field in the tracking volume has never been measured, and the discrepancy between the actual field and modeled field is unknown. Although there is no evidence of any mis-modeling of the solenoid field, we increase the field by 0.02%, which is larger than the measured uncertainty of the field, 0.013% (0.2 mT). The simulation of the SVT material is believed to be accurate to within 4.5%, but the increase we use is substantially larger. To account for the uncertainty of the momentum reconstruction we add the mass shifts originating from these corrections in quadrature. This results in the dominating systematic uncertainty of ± 0.39 MeV. The systematic uncertainties are summarized in Table V.

Another important source of systematic error comes from the uncertainty in the absolute scale of the e^+e^- CM energy. From the error propagation of Eq. (2), we find

$$\delta(M_p) = \frac{E_h^* - P_h^*}{M_p} \delta(\sqrt{s}/2). \quad (4)$$

Near the endpoint of the pseudomass distribution, $E_h^* \approx \sqrt{s}/2$, and $M_h^* \approx M_\tau$, so that $\delta(M_\tau) \approx 0.17\delta(\sqrt{s}/2)$.

The e^+e^- CM energy calibration has been seen to drift over time due to changing beam conditions. Over a two-year period of data taking, the calibration had drifted by -2.6 MeV. We exploit the fact that the $\Upsilon(4S)$ resonance decays exclusively to $b\bar{b}$ pairs and calibrate $\sqrt{s}/2$ based on the measured invariant mass of fully reconstructed B meson decays using the equation

$$M_B = \sqrt{(\sqrt{s}/2)^2 - P_B^{*2}}, \quad (5)$$

where M_B and P_B are the mass and reconstructed momentum of the B meson. We reconstruct a dozen hadronic B decay modes and divide the data into subsamples of 2500 candidates each. We then perform a maximum-likelihood fit to the reconstructed mass distribution for each subsample to extract the central value of M_B and then adjust $\sqrt{s}/2$ to obtain the world average B meson mass [8]. We apply this correction to the value of $\sqrt{s}/2$ for all data taken during the time period corresponding to each subsample. The statistical uncertainty of this correction is negligible, so the only uncertainty in $\sqrt{s}/2$ is due to the error in the PDG average value of the B meson mass (0.5 MeV) [8]. This

uncertainty in $\sqrt{s}/2$ corresponds to a systematic uncertainty in M_τ of 0.09 MeV.

Since we have a limited number of MC events, there are statistical errors associated with the straightline fit parameters a_0 and a_1 (Fig. 3). These errors introduce a systematic error in M_τ of ± 0.05 MeV.

We also consider alternatives for the pseudomass fit parametrization [Eq. (3)], by fitting with two other functions [11]:

$$F_1(M_p) = (p_3 + p_4 M_p) \frac{M_p - p_1}{\sqrt{p_2 + (M_p - p_1)^2}} + p_5 + p_6 M_p \quad (6)$$

and

$$F_2(M_p) = (p_3 + p_4 M_p) \frac{-1}{1 + \exp\frac{M_p - p_1}{p_2}} + p_5 + p_6 M_p. \quad (7)$$

We repeat the fitting procedure with F_1 and F_2 and obtain shifts in M_τ of -0.02 MeV and $+0.02$ MeV, respectively. We add the shifts in quadrature and find ± 0.03 MeV as the systematic uncertainty.

We also investigate the choice of fit range. We applied the procedure discussed in Sec. III using toy MC samples, refitting each sample with various fit ranges. We take the largest shift, 0.05 MeV, as the systematic uncertainty.

We study the effect of the MC modeling of the three-pion mass distribution in tau decays. We find that the peak of the distribution in MC is about 300 MeV lower than that in the data, while the widths of the distributions are similar. The MC modeling for the $\tau^- \rightarrow \pi^- \pi^+ \pi^- \nu_\tau$ and its charge conjugates is based on 16 form factors [24] determined from low statistics data from the LEP and CLEO experiments: measuring the form factors is a very challenging task that has not yet been performed on the high statistics data collected by *BABAR*. Although there is this discrepancy, we find that the pseudomass distribution in MC is similar to that in data. To test for possible effects in the endpoint of the pseudomass distribution due to the modeling of the 3π invariant mass, we generate four toy MC samples, varying the mean and width of the 3π mass by ± 300 MeV. We find that the shifts in the pseudomass endpoint are consistent with zero, but we conservatively take the average of these shifts, 0.05 MeV, as the systematic uncertainty due to the MC modeling.

We also investigate the choice of background estimation and pion misidentification and find the effects on the fit result are negligible. We also find the error due to the uncertainty in the boost of the CM frame and the uncertainty in the MC modeling of the track resolution to be negligible.

We have assumed that the neutrino mass is zero even though the PDG limit for the direct measurement is $M_{\nu_\tau} <$

18.2 MeV [8]. Neutrino experiments [25] have measured differences in the mass squared between the three neutrinos to be much less than 1 eV^2 [26]. Direct measurements of $M_{\nu_e} < 2 \text{ eV}$ [8] thus suggest that the mass of the τ neutrino is $\mathcal{O}(<1 \text{ eV})$. We perform MC studies on the effect of the neutrino mass on the τ mass determination and find that a 1 MeV neutrino mass would bias our result by -0.02 MeV.

All of the systematic effects listed above cancel in the τ^+ and τ^- mass-difference measurement. An additional systematic arises from the possible charge asymmetry discussed in Sec. IV D. To study this effect, we measure the mass differences for charged D and D_s mesons, which are presented in Table VI. We take a weighted average of the absolute values of the mass differences, 0.06 MeV, as the resulting systematic uncertainty. As a cross check of the τ sample, we studied the mass difference $M_{\tau^+} - M_{\tau^-}$ separately for the e and μ tags, before and after the 20% increase of the SVT material, and find consistent results.

VII. CONCLUSIONS

In summary, we have measured the mass of the tau lepton to be $1776.68 \pm 0.12(\text{stat}) \pm 0.41(\text{syst})$ MeV, where the main source of uncertainty originates from the uncertainty in the reconstruction of charged particle momenta. This result is in agreement with the world average [8].

We measure the mass difference of the τ^+ and τ^- to be $-0.61 \pm 0.23(\text{stat}) \pm 0.06(\text{syst})$ MeV, or $(M_{\tau^+} - M_{\tau^-})/M_{\text{AVG}}^\tau = (-3.4 \pm 1.3(\text{stat}) \pm 0.3(\text{syst})) \times 10^{-4}$. We use our result to calculate an upper limit on the mass difference, $|M_{\tau^+} - M_{\tau^-}|/M_{\text{AVG}}^\tau < 5.5 \times 10^{-4}$ at 90% C.L. We find our measurement is consistent with the previously published results made by the Belle Collaboration. We perform parametrized MC studies to determine the significance of our result of the mass difference. We generate 4500 samples each for the τ^+ and τ^- with the masses of each sample set to the value extracted from the combined data sample, 1776.68 MeV. The samples are generated with the same number of events as the number of events in the data. We fit each sample and calculate the mass difference between the τ^+ and τ^- samples. We also repeat the procedure using an alternative parametrization [Eq. (6)], and determine that the two parametrizations give consistent results. We find, assuming no *CPT* violation, that there is a 1.2% chance of obtaining a result as different from zero as our result.

ACKNOWLEDGMENTS

We are grateful for the extraordinary contributions of our PEP-II colleagues in achieving the excellent luminosity and machine conditions that have made this work possible. The success of this project also relies critically on the expertise and dedication of the computing organ-

izations that support *BABAR*. The collaborating institutions wish to thank SLAC for its support and the kind hospitality extended to them. This work is supported by the US Department of Energy and National Science Foundation, the Natural Sciences and Engineering Research Council (Canada), the Commissariat à l’Energie Atomique and Institut National de Physique Nucléaire et de Physique des Particules (France), the Bundesministerium für Bildung und Forschung and Deutsche Forschungs-

gemeinschaft (Germany), the Istituto Nazionale di Fisica Nucleare (Italy), the Foundation for Fundamental Research on Matter (The Netherlands), the Research Council of Norway, the Ministry of Education and Science of the Russian Federation, Ministerio de Educación y Ciencia (Spain), and the Science and Technology Facilities Council (United Kingdom). Individuals have received support from the Marie-Curie IEF program (European Union) and the A. P. Sloan Foundation.

-
- [1] J.Z. Bai *et al.* (BES Collaboration), *Phys. Rev. D* **53**, 20 (1996).
 - [2] Y. Tsai, *Phys. Rev. D* **4**, 2821 (1971).
 - [3] W.J. Marciano and A. Sirlin, *Phys. Rev. Lett.* **61**, 1815 (1988).
 - [4] J. Schwinger, *Phys. Rev.* **91**, 713 (1953).
 - [5] J. Schwinger, *Phys. Rev.* **94**, 1362 (1954).
 - [6] G. Lüders, K. Dan. Vidensk. Selsk. Mat. Fys. Medd. **28N5**, 1 (1954).
 - [7] W. Pauli, *Niels Bohr and the Development of Physics* (Pergamon Press, Elmsford, NY, 1955).
 - [8] C. Amsler *et al.*, *Phys. Lett. B* **667**, 1 (2008).
 - [9] S. Banerjee, B. Pietrzyk, J.M. Roney, Z. Was, *Phys. Rev. D* **77**, 054012 (2008).
 - [10] H. Albrecht *et al.* (ARGUS Collaboration), *Phys. Lett. B* **292**, 221 (1992).
 - [11] K. Belous *et al.* (Belle Collaboration), *Phys. Rev. Lett.* **99**, 011801 (2007).
 - [12] V.V. Anashin *et al.* (KEDR Collaboration), *Nucl. Phys. B, Proc. Suppl.* **169**, 125 (2007).
 - [13] G. Abbiendi *et al.* (OPAL Collaboration), *Phys. Lett. B* **492**, 23 (2000).
 - [14] D.J. Lange, *Nucl. Instrum. Methods Phys. Res., Sect. A* **462**, 152 (2001).
 - [15] T. Sjöstrand, S. Mrenna, and P. Skands, *J. High Energy Phys.* **05** (2006) 026.
 - [16] B.F.L. Ward, S. Jadach, and Z. Was, *Nucl. Phys. B, Proc. Suppl.* **116**, 73 (2003).
 - [17] S. Jadach, Z. Was, R. Decker, and J.H. Kuhn, *Comput. Phys. Commun.* **76**, 361 (1993).
 - [18] E. Barberio and Z. Was, *Comput. Phys. Commun.* **79**, 291 (1994).
 - [19] S. Agostinelli *et al.* (GEANT4 Collaboration), *Nucl. Instrum. Methods Phys. Res., Sect. A* **506**, 250 (2003).
 - [20] B. Aubert *et al.* (*BABAR* Collaboration), *Nucl. Instrum. Methods Phys. Res., Sect. A* **479**, 1 (2002).
 - [21] G. Benelli, K. Honscheid, E. A. Lewis, J.J. Regensburger, and D.S. Smith in 2006 IEEE Nuclear Science Symposium Conference Record, Vol. 5, (IEEE, San Diego, CA, 2006), p. 1470.
 - [22] D. Brown, E. Charles, and D. Roberts, *The BABAR Track Fitting Algorithm* (Padova, Italy, 2000).
 - [23] B. Aubert *et al.* (*BABAR* Collaboration), *Phys. Rev. D* **72**, 052006 (2005).
 - [24] J.H. Kuhn and E. Mirkes, *Z. Phys. C* **56**, 661 (1992).
 - [25] D. Karlen, *Phys. Lett. B* **667**, 1 (2008).
 - [26] P. Vogel and A. Piepke, *Phys. Lett. B* **667**, 1 (2008).